

Lignin-Based Direct Ink Printed Structural Scaffolds

Bo Jiang, Yonggang Yao, Zhiqiang Liang, Jinlong Gao, Gegu Chen, Qinqin Xia, Ruiyu Mi, Miaolun Jiao, Xizheng Wang, and Liangbing Hu*

3D printing of lignocellulosic biomass (cellulose, hemicellulose, and lignin) has attracted increasing attention by using this abundant, sustainable, and ecofriendly material. While cellulose can be easily tailored into a highly viscous ink for 3D printing, after solvent evaporation, the final printed structures become highly porous, fragile, and easily fall apart in water due to its hydrophilic nature. Lignin, another crucial component of natural lignocellulose, has not yet been reported for ink printing due to its unfavorable rheological behavior. Herein, a low-cost direct ink printing strategy is developed to fabricate lignin-based 3D structures with lignin no further refined and a more compact microstructure as well as different functionalities compared with printed cellulose. By using a soft triblock copolymer as the crosslinking agent, the rheology of lignin-based inks can be adjusted from soft to rigid, and even enables vertical printing which requires stiff and self-supporting features. The lignin-based inks contain less water (≈ 40 wt%) and exhibit a much denser, stiffer structure, resulting in a wet tensile strength of ≈ 30 MPa, compared to only ≈ 0.6 MPa for printed cellulose. In addition, the unique macromolecular structure of lignin also demonstrates significantly improved stability in water and under heat, as well as UV-blocking performance.

1. Introduction

3D printing, also referred to as additive manufacturing, is a state-of-the-art prototyping technic that can rapidly create diverse structures for a range of applications, such as biomedical scaffolds, functional materials and energy storage systems.^[1–7] However, most 3D printing techniques use non-biodegradable or petroleum-based plastic products such as acrylonitrile butadiene styrene (ABS), polyamide, polycarbonate and epoxy resins,^[8] which will be a large threat to our environment and human health especially when scaled up. Therefore, a sustainable, biodegradable, ecofriendly, and low-cost plastic replacement is urgently needed. Recently, 3D printing of lignocellulosic biomass (cellulose, hemicellulose, and lignin) has attracted increasing attention as these materials are abundant,

cost-efficient, ecofriendly, and biodegradable.^[9–11] Wood is the most abundant natural resource for lignocellulosic biomass and contains a combination of cellulose (30–50%), hemicellulose (15–30%), and lignin (20–35%).^[12,13] As a main constituent in natural wood, cellulose has excellent water retention capability due to its hydrogen bonding network, which allows it to be easily tailored into a highly viscous ink for 3D printing.^[14–19] However, printed cellulose structures are vulnerable to various environmental factors, leading to disadvantages such as structural instability in humidity and water, poor wet strength, ultraviolet (UV) radiation aging.^[20] Importantly, after water evaporation (>90 wt%), the final printed cellulose structures become highly porous, fragile, and easily fall apart in water, which is undesirable for application as a mechanical support or scaffold.

On the other hand, lignin, another crucial part of lignocellulose, demonstrates various attractive material properties, including high stiffness, excellent water stability, UV-blocking capability, and thermostability,^[21,22] which could provide different functionalities and applications compared with cellulose-based materials. In addition, lignin is produced on a massive-scale in industry, such as paper mills, making it a byproduct and inexpensive material. Therefore, developing a strategy to fabricate 3D structures of lignin via a facile and scalable method could be an important contribution for value-added biomass utilization and also broaden the material, structure, and function choices for 3D biomass devices. Although fused deposition modeling (FDM) was previously used for melt printing of kraft and organosolv lignin,^[23–25] this printing technology is heavily dependent on the molecular structures of lignin, particularly those with linear syringyl units from hardwood and oligomeric fraction of extracted softwood lignins, thus requiring their refinement and increasing the material and processing costs. Moreover, as an energy-consuming process, FDM requires molten lignin at a high temperature (>170 °C), which can degrade the material into a rigid char, and the remediation by adding nylon^[25] and ABS^[26] often leads to the resultant 3D printed structure showing poor thermal stability and being very brittle.^[27,28] Currently, direct ink printing, with the key advantages of the flexibility of material selections and room temperature processing environment, has not yet been reported for lignin due to its rigid structure and poor water retention,

Dr. B. Jiang, Dr. Y. Yao, Prof. Z. Liang, J. Gao, G. Chen, Q. Xia, R. Mi, M. Jiao, Dr. X. Wang, Prof. L. Hu
Department of Materials Science and Engineering
University of Maryland
College Park, MD 20742, USA
E-mail: binghu@umd.edu

 The ORCID identification number(s) for the author(s) of this article can be found under <https://doi.org/10.1002/smll.201907212>.

DOI: 10.1002/smll.201907212

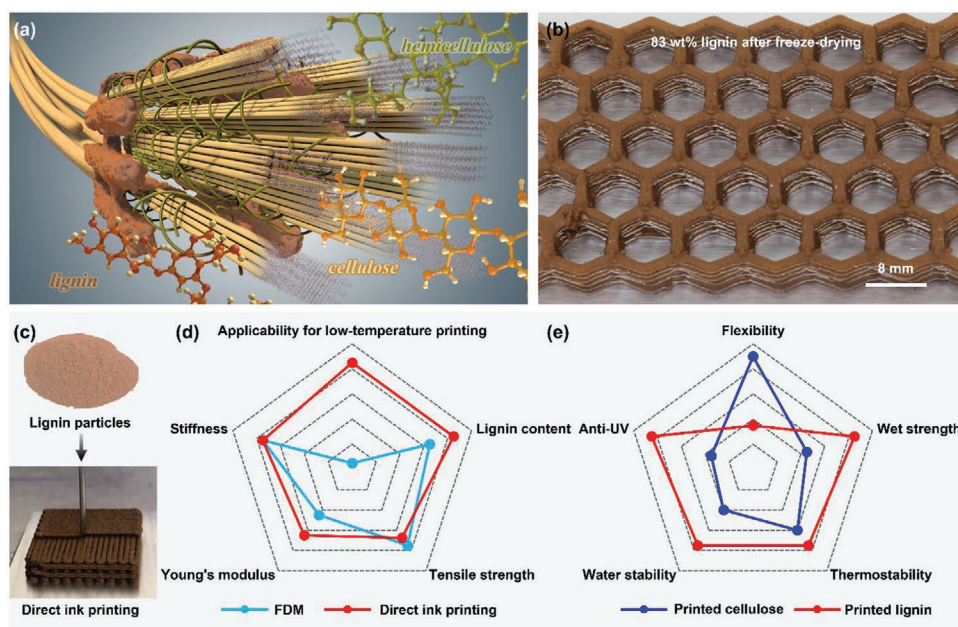


Figure 1. a) Schematic of the structural composition (cellulose, hemicellulose, and lignin) of natural wood. b) Image of a resulting 3D-structure of lignin featuring a honeycomb pattern. c) Digital images of lignin particles obtained from pulp mills and the direct printing of the lignin-based ink. The lignin particles are transformed into a printable ink that can be steadily extruded as a filament and integrated into a 3D structure through a layer-by-layer manner. d) A radar chart compares the various properties of 3D printed lignin-based structure by FDM and direct ink printing. e) A radar chart compares the various properties of 3D printed lignin and cellulose.

resulting in an unfavorable ink rheology for printing. Additionally, lignin obtained from pulping engineering exists in a loose particulate state. These particles have low interaction with each other and the aqueous solvent (due to lignin's poor hydrophilicity), further challenging direct ink printing of this material.

Herein, inspired by the wood structure that lignin a natural binder, contributing to the strength, water stability and rigidity of the cell walls (Figure 1a), we developed a low-cost direct ink printing strategy to build lignin-based 3D structures, which offer different functionalities compared with printed cellulose. We adopt a facile two-step approach to prepare the printable lignin-based inks, which involves 1) mechanical ultrasonication in water and 2) chemical crosslinking with Pluronic F127. The ultrasonication breaks down the large, irregular particles of lignin into small particles, which promotes smooth printing. The chemical crosslinking step through the addition of the soft triblock copolymer F127 improves the rheological and viscoelastic properties of the inks, allowing them to be extruded from a syringe needle via direct ink printing for constructing 3D structures (Figure 1b,c). This successful direct ink printing of lignin shows many advantages over FDM,^[25] such as low-temperature printing (25 °C versus >170 °C) to avoid structural deterioration at high temperature, higher lignin content in resultant materials (83 wt% versus 40–60 wt%) which lead to a higher Young's modulus (5.0 GPa vs 3.01 GPa) in the printed structures (Figure 1d). Compared with printed cellulose, the 3D printed lignin displays added and even advanced properties of high stiffness, thermostability, water stability and UV-blocking performance (Figure 1e). Moreover, this new approach allows the direct ink printing of lignin to produce various 3D structures and is not dependent on the molecular structure of lignin,

thus offering a greener and sustainable material for 3D printing toward high-performance structures. We anticipate this technique could also largely broaden the value-added applications of this cost-effective and ecofriendly material, which originally is treated as the industrial waste.

The development of viscoelastic ink with optimum rheological behavior that can be readily extruded and form a self-supporting framework is the key to fabricating desired 3D patterns through direct ink printing. The molecular structure and morphology of lignin are the main factors affecting its viscoelasticity and printability. For example, alkali lignin from hardwood mainly consists of guaiacyl and syringyl units (with minor *p*-hydroxyphenyl units), and that from softwood is mainly composed by guaiacyl units (with minor syringyl and *p*-hydroxyphenyl units) (Figure S1a,b, Supporting Information). In addition, the hardwood lignin exhibits higher content of β -aryl ether bonds (β -O-4') and lower condensation degree (β - β' and β -5') than softwood lignin (Figure S1c, Supporting Information). The structural differences between them result in different printing rheological behavior.^[25] Therefore, it is necessary to evaluate the universality of direct ink printing for different lignins. Unlike cellulose, directly mixing lignin with water results in unfavorable rheological properties that prevent printing. Generally, lignin directly obtained from pulping mill has an inhomogenous particle size of 0–60 μ m (Figure S2a,b, Supporting Information), which easily causes the blocking of the printing nozzle. Ultrasonication is an effective and facile method to make the lignin particles smaller with the diameter distribution of 0–8 μ m (Figure S2c,d, Supporting Information). However, the rheological behavior of lignin is mainly controlled by its inherent structure, the rigid phenylpropane

units and poor water retention of lignin still cause it to separate from water under high shear stress (Figure 2a,b). As a result, the lignin mixed with water tends to clog the printing nozzle. Therefore, a wetting agent is necessary to improve the printability of such lignin inks. In this work, we added Pluronic F127 aqueous solution to crosslink lignin with different formulations in order to form a highly viscous ink (Figure 2c). The terminal hydroxyl groups of F127 endow the resulting ink with high water retention and the outstanding rheological properties of F127 addresses the rigid structure of lignin by wrapping the lignin particles into the F127 matrix (Figure 2d), forming a flexible gel at room temperature. Moreover, the hydrophilicity of F127 has been demonstrated that can provide a better adhesion

for printed structure.^[29] Therefore, the resulting viscoelastic ink can be steadily squeezed out from a syringe as a continuous filament (Figure 2e) even without further particle refining to lignin, a necessary characteristic for low-cost 3D printing processes.

We conducted a series of rheology measurements to quantitatively understand how the printability of the lignin/F127/water ink compares with the lignin/water formulation. The lignin/water and lignin/F127/water inks with a lignin concentration of 50 wt% (containing water) both display a viscoelastic behavior with a large shear yield strength in the storage moduli G' (Figure 2f) and a pronounced linear decrease in the viscosity (Figure 2g). Although a large storage modulus G' (10^6 Pa) and

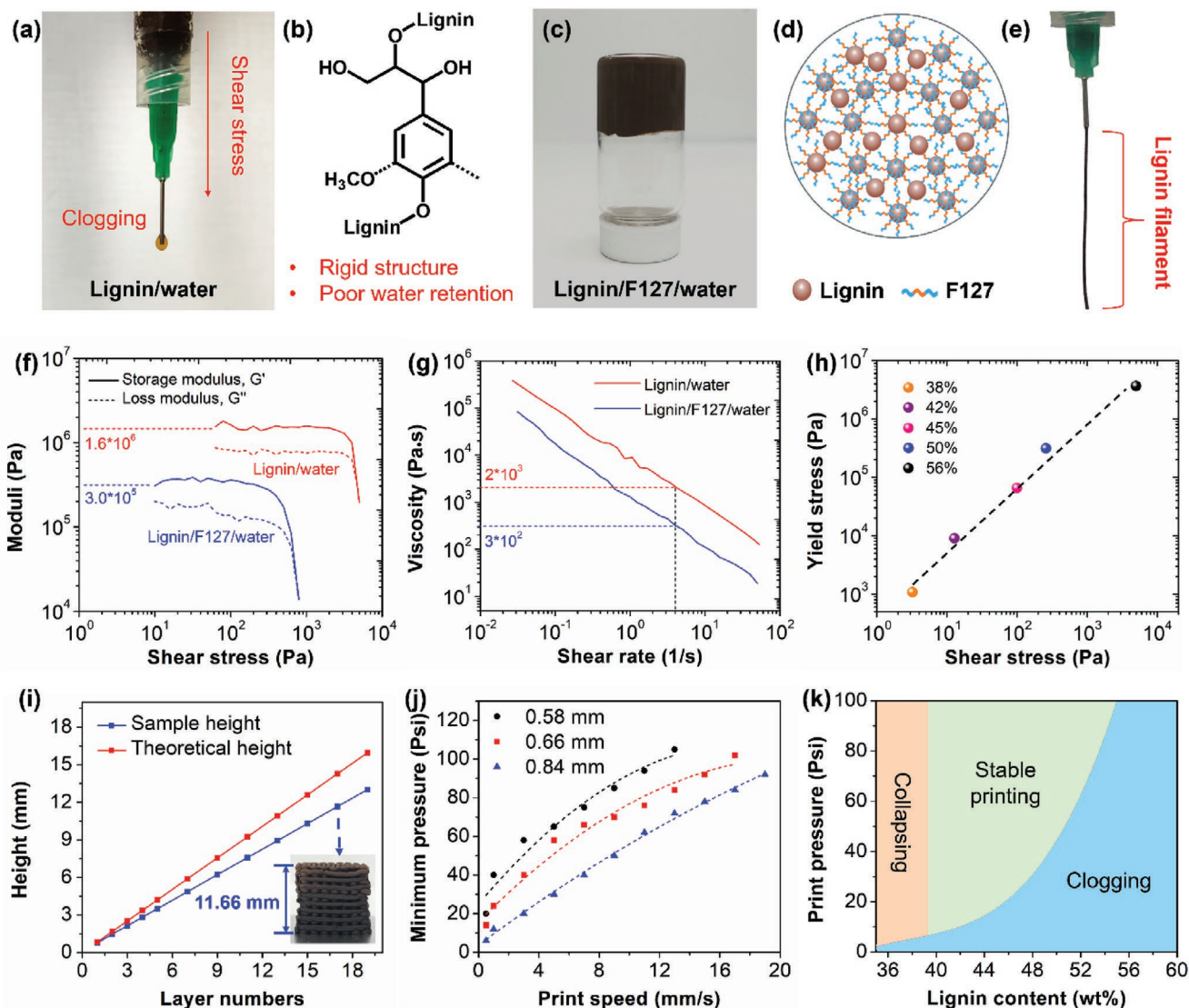


Figure 2. a) A digital image of the lignin/water ink and b) schematic of the lignin structural unit. The rigid phenylpropane structure and poor water retention result in poor ink flow. c) Digital image of the lignin/F127/water ink (with 50 wt% of lignin) stored in an inverted vial to demonstrate its high viscosity. d) Schematic of the interaction of lignin with F127. e) Digital image of a lignin/F127/water filament extruded out from a syringe with clearly improved lignin printability. f) The storage (G') and loss moduli (G'') as a function of shear stress and g) the apparent viscosity as a function of shear rate for the lignin/water and lignin/F127/water inks. h) The yield point of the lignin/F127/water inks at different concentrations. i) Shape retention of the printed structure as a function of layer number. j) The relationship between the printing speed and the minimum pressure for different diameter needles. k) Regions of stable (light green) and unstable (light blue and orange) printing for lignin/F127/water inks.

high viscosity are good for retaining the filamentary shape in 3D printing, the inherent poor water retention and rigid structure of lignin for lignin/water ink results in a huge frictional resistance of lignin particles under shear stress, making it difficult to be easily extruded out from a nozzle.^[30] Due to the crosslinking of lignin using the F127 gel, the lignin/F127/water ink displays excellent rheological behavior (flow property and water retention) and a much lower yield stress of ≈ 3000 Pa than lignin/water ink, which should support successful ink printing. In addition, the moduli and viscosity of the lignin/F127/water ink can be readily adjusted by changing the lignin concentration (38–56 wt%, Figure S3, Supporting Information), and the yield stress and corresponding shear stress show a good linear relationship within the experimental concentrations studied (Figure 2h). The well-controlled rheological behavior indicates that the shear stress is easily up to the yield point to overcome the friction resistance of particle–particle bonds of lignin for printing.

As shown in Video S1 (Supporting Information), the lignin filament continuously and steadily flows through the nozzle and demonstrates an outstanding self-supporting capacity that enables it to form a 3D-structure. After freeze-drying, the 3D printed pattern of lignin well maintains its integrity with negligible change (Figure S4, Supporting Information). We also verified the shape retention capability of the 3D printed lignin structure, particularly in the thickness direction where fragile filaments can easily collapse. For this printing experiment, a single layer of the printed filament featured a thickness of 0.78 mm. As shown in Figure 2i, the printed lignin layers display only a slight deviation from the theoretical height: the printed grid pattern has a thickness of 2.13, 4.86, 8.94, and 11.66 mm for 3, 7, 13, and 17 layers, respectively, indicating the relatively stiff structure of our printed lignin which prevents structural collapse during and after printing. The sharp retention capability of the designed 3D patterns is governed not only by the rheological properties of the ink but also by various parameters, such as the diameter of the needle, the printing speed, the printing pressure, the interval between the extrusion lines, and the printing pathway.^[23,31] Therefore, mapping a stable printing region is important for the direct ink printing of lignin. First, we determined the relationship between the printing speed and the required minimum pressure for different inner diameters of needles (Figure 2j). The printing pressure increases with printing speed and a nearly linear relationship between them is observed for different needle diameters. In addition, we also mapped the lignin concentration (35–60 wt%) on the stable ink printing (Figure 2k). Within the pressure range of 0–100 psi, the lignin inks clog at a high concentration (>56 wt%) and the printed grid structure collapses at a lower concentration (<38 wt%). Although the β -O-4' linkages in the lignin structure offer some flexibility, the condensed structure of the biphenyl and biphenyl ethers from the guaiacyl and *p*-hydroxyphenyl units and the considerable steric hindrance from the syringyl units weaken the flow behavior of the lignin inks.^[25,32] As a result, at higher concentration, this rigid molecular structure of lignin dominates and diminishes the ink's smooth flow, thus diminishing the material's printability. On the other hand, with lower concentration, the soft additive (F127 aqueous solution) leads to a highly mobile lignin ink, causing the collapse of the

lignin filaments, preventing construction of stable 3D structures. However, within the concentration range of 38–56 wt% lignin, the inks readily flow through the nozzle and are also highly adjustable from soft to rigid to form diverse sophisticated patterns with the adjacent layers tightly bonded (Figure S5, Supporting Information), which we attributed the adhesion between the 3D printed layers to the hydrogen-bond interaction,^[28] especially considering the gravitational force that helps the close contact and bond formation. Moreover, we also demonstrated that this direct ink strategy is not dependent on lignin types or their molecular structures, with all alkali and kraft lignins (water insoluble) from hardwood and softwood showing excellent printability (Figure S6, Supporting Information).

We observed the detailed structure of the printed lignin-based filament under microscopy (Hitachi SU-70) and compared it with that of printed cellulose. As shown in Figure 3a,b, the lignin particles (<8 μm) are distributed in the printed filament and wrapped by the F127 gel, making the whole filament an integral structure—drastically different from previous loose particulate forms (Figure 1c). In contrast, the printed cellulose shows a highly porous structure after freeze-drying (Figure 3c) due to the enormous amount of water in the cellulose ink (>90 wt%). Figure 3d summarizes the composition of the cellulose ink and our lignin-based ink after printing and freeze-drying to further illustrate the differences between these materials. Cellulose features a linear structure with abundant hydroxyl groups that can form strong hydrogen bonding interactions with water, which endows cellulose ink with excellent water retention and property of shear thinning (Figure S7a, Supporting Information) for direct ink printing. By adjusting the water content, cellulose can be easily tailored into a highly viscous ink with an adequate storage modulus and yield stress (Figure S7b, Supporting Information). Yet, the water content in the cellulose ink is often higher than 90 wt% to maintain printability, otherwise it will cause the agglomeration of cellulose fibers and clog at the printing nozzle and such a highly water content makes the resultant structure highly fragile after evaporation. In contrast, our lignin ink only contains less than 40 wt% of water for printing, which gives the printed filament a much denser structure after water evaporation. Further analysis shows that the printed cellulose has a porous structure with the specific surface area of 106.0 m^2 g^{-1} , much higher than freeze-dried lignin filament (45.7 m^2 g^{-1} , Figure S8, Supporting Information). Compared with FDM, the 3D-structure fabricated by direct ink printing contains 83 wt% lignin in the resultant materials, which is much higher than that printed by FDM (40–60 wt%).^[25]

The differences in ink composition and final printed structures lead to different properties for the lignin and cellulose materials, particularly mechanical ones. Aside from a dense structure, the biphenyl, biphenyl ethers, and aromatic methane carbons in lignin also serve as stiff segments that endow the printed filament with high stiffness. For example, we demonstrate that the lignin filament can be printed and suspended on a substrate with a large span gap (18 mm) and well maintain its shape without collapsing or breaking after printing. However, the corresponding printed cellulose filament fractures under the internal shrinkage stress due to the weak interaction between the wet cellulose fibers (Figure 3e). The printed lignin filament can even support itself from just one end even

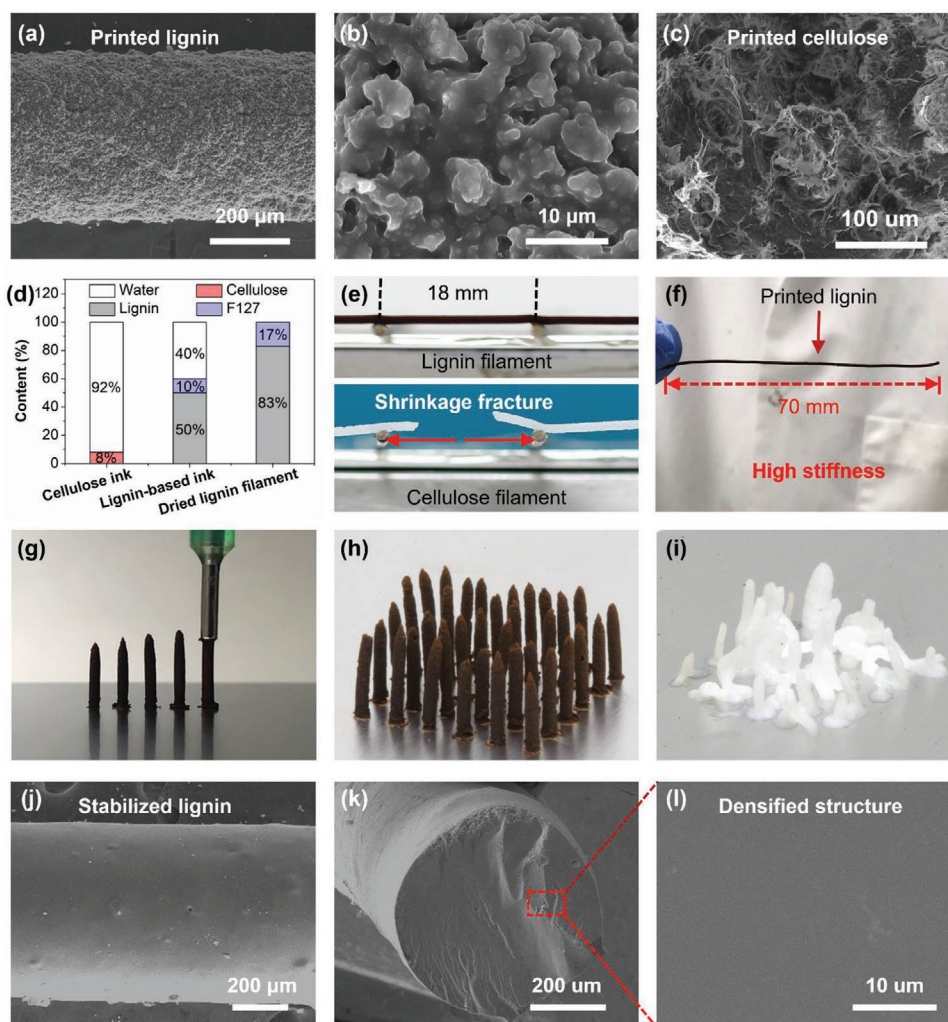


Figure 3. The printed lignin filaments compared with printed cellulose filaments. a,b) The surface topography of the printed lignin filament. The lignin particles are crosslinked and wrapped by F127 with a dense structure. c) The surface topography of the printed cellulose to show the porous structure. d) The composition of the cellulose ink, our lignin ink after printing and freeze-drying. e) The suspended lignin and cellulose filaments over a grooved substrate at ambient temperature. The printed lignin has high stiffness that can well maintain its shape, while the printed cellulose fractures under the internal shrinkage stress. f) Image of the printed lignin filament that can support itself at one end. g,h) Images of the vertical printing of lignin and i) cellulose. Cellulose cannot form a free-standing structure via vertical printing. j–l) The surface and cross-sectional scanning electron microscope (SEM) images of the thermally stabilized printed lignin filament, demonstrating its densified structure.

for a very long filament (>70 mm), demonstrating both strong and stiff mechanical properties (Figure 3f). The high stiffness of the lignin-based ink is critical for shape retention and construction of complex 3D structures requiring outstanding self-supporting capacity. We successfully demonstrated vertical printing of lignin enabled by the stiffness of the printable ink (Figure 3g,h), in which the height of the printed lignin filament is adjustable and can be as high as 20 mm (Figure S9, Supporting Information). Meanwhile, the cellulose ink cannot be vertically printed due to the poor mechanical robustness of the printed filaments (Figure 3i).

The printed lignin-based structures can be further improved by enhancing the interaction between the lignin particles through a low temperature (120 °C) air-stabilization process. Due to the reverse thermoresponsive property,^[33,34] F127 at a such temperature will become a gel, which helps to maintain

the 3D matrix of the printed filament and prevent structural collapse during the thermal stabilization process. Additionally, lignin has a low glass transition temperature (80–150 °C)^[35–37] and can easily melt into a homogenous material, through which the previous particle-particle structure in lignin will become a dense, integral 3D, interconnected structure, eliminating most particle interfaces (Figure 3j–l). After thermal stabilization, the printed lignin filament become more denser with the specific surface area of 2.3 m² g⁻¹, ≈20 times lower than that before thermal stabilization (Figure S8, Supporting Information). Moreover, the thermal stabilization maintains the structural integrity of lignin without obvious degradation, as demonstrated by Fourier transform infrared (FTIR) spectroscopy (Figure S10, Supporting Information), with the typical absorption bands of hardwood lignin's aromatic rings clearly observed at 1592 cm⁻¹ (guaiacyl) and 1512 cm⁻¹ (syringyl) after

the thermal treatment.^[38] Such a facile and effective low temperature stabilization process physically melts the particles into an interconnected structure, which should largely improve the mechanical performance and water stability of the printed lignin-based 3D structures.

The densified structure and the unique molecular structure of lignin endow the printed lignin 3D structures with

outstanding performance superior to that of printed cellulose. For example, the homogenous structure formed by thermal stabilization and the hydrophobicity of lignin allow the printed structure to well maintain its integrity in water under stirring (Figure 4a), while the corresponding cellulose structure is easily decomposed into microfibrils (Figure 4b). Such water stability is critical for practical applications, which often involve humidity

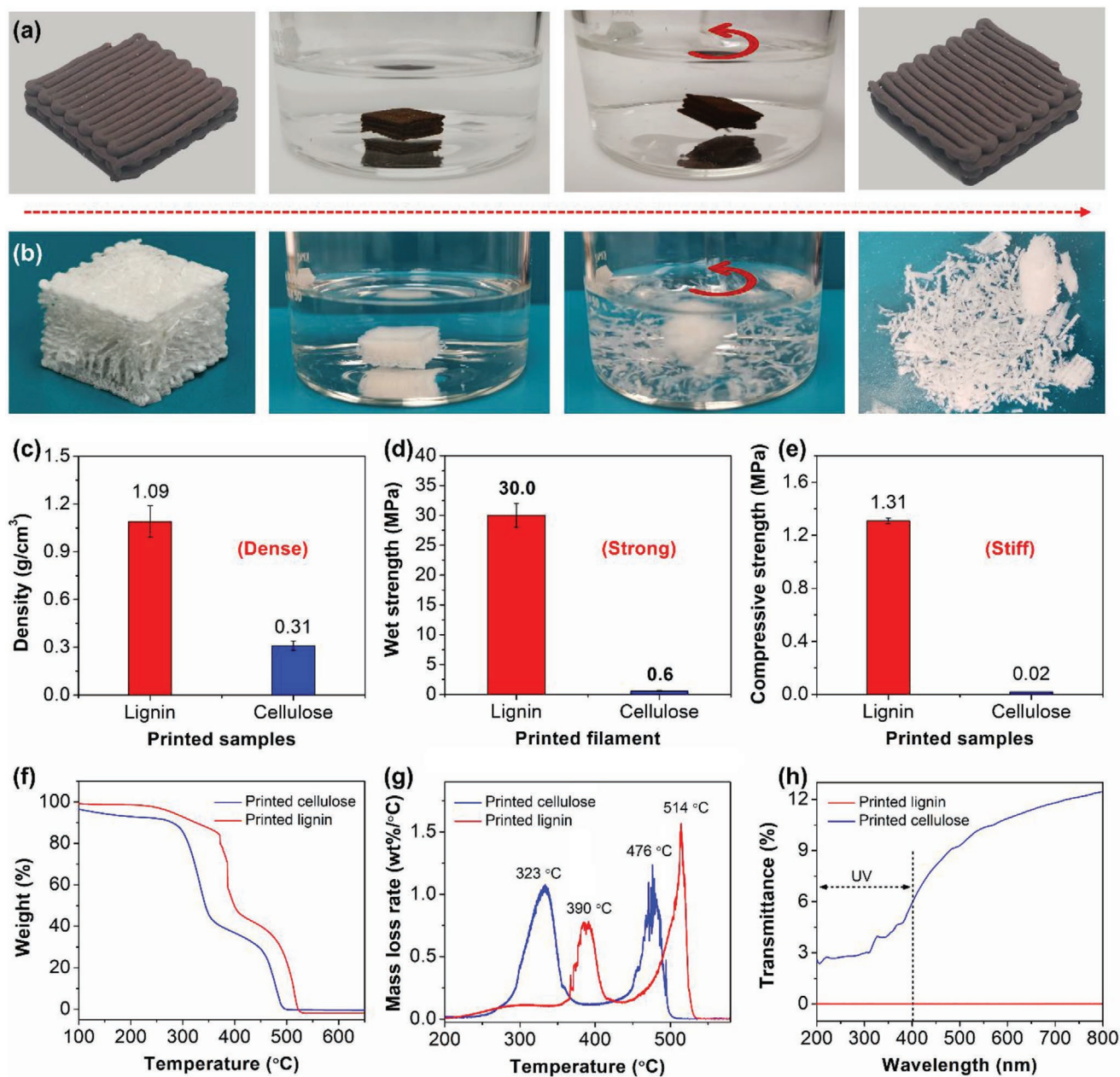


Figure 4. The high performance of the thermally stabilized printed lignin compared with that of printed cellulose. Water stability characterization of a) the thermally stabilized 3D-structure of lignin and b) printed cellulose. The thermally stabilized lignin can well maintain its integrity, but the printed cellulose falls apart in water. c) The density of the thermally stabilized lignin and cellulose, in which the thermally stabilized lignin shows a denser structure. d) The wet strength of a printed single filament of the thermally stabilized lignin and printed cellulose filament. The thermally stabilized lignin filament shows higher wet tensile strength than the corresponding cellulose filament. e) The compressive strength of the thermally stabilized lignin and cellulose at a strain of 2%. Thermally stabilized lignin shows higher rigidity. The f) weight loss and g) mass loss rate of the thermally stabilized lignin and cellulose. h) The UV transmittance curves of the thermally stabilized lignin and cellulose, in which the printed lignin shows excellent UV-blocking performance.

and water-based solvents, especially for materials used in biomedical applications. The printed lignin is capable of achieving a high density of 1.09 g cm^{-3} , while the printed cellulose only shows a low density of 0.31 g cm^{-3} (Figure 4c), which in many cases is too light and fragile to serve as an effective 3D scaffold or support. The lignin filament after thermal stabilization shows a considerable wet tensile strength of $\approx 30 \text{ MPa}$ (with the Young's modulus of 5.0 GPa) while the printed cellulose demonstrates only $\approx 0.6 \text{ MPa}$ (Figure 4d). Additionally, the compressive strength of the 3D printed lignin structure is also higher than that of cellulose (Figure 4e).

We believe the water stability and mechanical reinforcement of the lignin filament is a synergistic effect from its dense structure, the interconnection of the lignin particles during thermal stabilization,^[37] and the rigid aryl molecular structures. Therefore, during thermal stabilization, the lignin particles melt and gradually disperse in the F127 matrix through strong intermolecular interactions, which meanwhile offers it a dense structure, preventing water from entering the interior of lignin filaments. Although the water soluble F127 is not conducive to the stability of printed 3D lignin structure in water, the homogeneous structure of lignin formed by thermal stabilization and the hydrophobicity of lignin can well maintain its integrity. On the other hand, more active sites are exposed on the lignin aromatic rings (especially for guaiacyl and *p*-hydroxyphenyl units) during thermal stabilization, facilitating the self-bonding of lignin structure through new C–C bonds, which endows the printed lignin structure with mechanical robustness. Our previous work has demonstrated that self-bonding occurs to lignin fragments during thermal treatment that the cleavage of β -aryl ether bonds induces the increase of condensed linkages of β - β , β -5', and β -1'.^[39] In contrast, during ink printing, the cellulose fibers are highly oriented under shear force (Figure S11, Supporting Information), giving the printed cellulose outstanding mechanical strength in the dry state (Figure S12, Supporting Information). However, the abundant hydroxyl groups on the cellulose fibers limits the application of printed cellulose in humid environments. Additionally, the lower compressive strength of the cellulose 3D structure is also not desirable for a scaffold that requires mechanical stiffness. Therefore, the outstanding wet tensile and compressive strength of the printed lignin display an added and even advanced properties to that of printed cellulose structure.

The structure of lignin is highly branched and amorphous, and mainly consists of *p*-hydroxyphenyl, guaiacyl, and syringyl units with various interunit linkages.^[12,22,40,41] These structural units and linkages give lignin many physicochemical and biological properties, such as thermostability, antioxidation, and anti-UV, that act as an advancement to the cellulose. For example, we demonstrate the thermostability and UV-blocking performance of printed lignin after thermal stabilization, as shown in Figure 4f–h. In terms of thermostability, both printed lignin and cellulose show a two-stage degradation curve over the interval of $250\text{--}500 \text{ }^\circ\text{C}$ (Figure 4f), but the maximum weight loss rate of the printed cellulose occurs at 323 and $476 \text{ }^\circ\text{C}$, while that of the printed lignin is higher at 390 and $514 \text{ }^\circ\text{C}$ (Figure 4g). Interestingly, the thermostability of the freeze-dried lignin 3D structure before thermal stabilization is higher than that of the original lignin particles (Figure S13,

Supporting Information), which demonstrates the occurrence of structural polymerization (chemical crosslinking) between the lignin and F127. F127 is a triblock copolymer with terminal hydroxy groups that can crosslink with the carboxyl at C_7 of the lignin structural units, which will increase the molecular weight of lignin, thereby improving its thermostability. Due to its phenolic hydroxyl groups, lignin also shows outstanding performance of UV absorption,^[21] resulting in 100% shielding of UV light (Figure 4h).

This successful 3D printing of lignin offers an attractive pathway for fast fabricating mechanically robust, thermally stable, and biocompatible 3D structures for a range of applications, including biomedical engineering and the energy-water nexus. Particularly, the direct ink printing could enable printing of lignin with other materials into a composite structure, for example, cellulose, ceramic powders, graphene, metal particles, etc., that are not applicable in FDM printing. Moreover, lignin as the second-abundant biopolymer in nature with the low cost and high carbon yield makes the printed 3D structure an ideal precursor for carbon materials. For example, we demonstrated that an activated carbon from lignin scaffold fabricated by a facile carbonization and activation process shows excellent performance on static adsorption of methylene blue (MB), much superior to the commercial activated carbon (Figure 5). After carbonization and activation, the activated carbon from printed lignin shows no obvious change on morphology, with the 3D scaffolds intact (Figure 5a). However, the dense structure of stabilized lignin become porous after carbonization and activation process (Figure 5b,c) with the density decreased from 1.09 to 0.28 g cm^{-3} . The oxygen and hydrogen from lignin are removed during this process, consequently introducing the porosity into the carbon structure,^[42] which has great potential for organic adsorption and environmental remediation. According to the standard adsorption curve shown in Figure S14 (Supporting Information), we measured the absorbance of MB solution at 665 nm after 20 min static adsorption by activated materials. From the UV–vis spectra in Figure 5d, the MB absorption peak almost disappeared for the activated carbon from printed lignin scaffold. Meanwhile, MB remains in solution for commercial activated carbon. Further analysis indicates that the removal efficiency of the activated carbon from lignin scaffold reaches 94.5%, while the efficiency is much lower for the commercial activated carbon (Figure 5e). Moreover, after fully adsorption, the adsorption capacity of the activated carbon from printed lignin is up to 124.6 mg g^{-1} , which is 2.48-times higher than the commercial activated carbon (Figure 5f). Therefore, the activated lignin carbon materials derived from this direct ink printing strategy show a highly efficient and economical replacement for commercial ones.

2. Conclusion

Inspired by the natural wood structure, we have developed a low-cost direct ink printing strategy to build lignin-based 3D structures, offering advanced properties of high stiffness, water stability, thermostability, and UV-blocking performance compared to printed cellulose. The rheological behavior of the lignin-based ink is highly adjustable by a wetting agent from

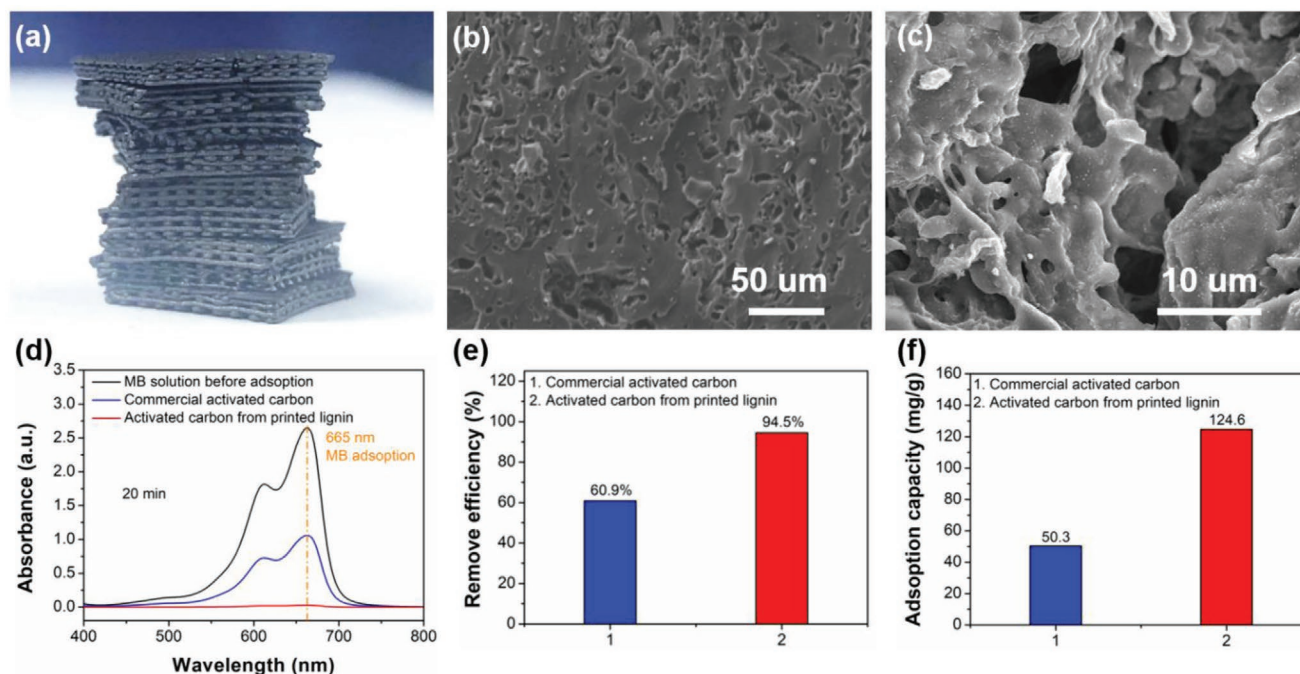


Figure 5. Activated carbon from printed lignin scaffold for water treatment. a) Image of activated carbon from printed lignin scaffold. b,c) Morphology of activated carbon from printed lignin scaffold. d) The UV-vis spectra of the MB solutions after 20 min adsorption by the activated carbon from printed lignin and commercial activated carbon. The typical adsorption peak of the MB is located at 665 nm. e) The removal efficiency for the static adsorption after 20 min for the active materials. f) The adsorption capacity of the commercial activated carbon and the activated carbon from printed lignin.

soft to rigid, and even enables vertical printing which requires stiff and self-supporting features. This successful 3D printing of lignin via a facile and scalable direct ink printing process offers an attractive pathway for fabricating mechanically robust, thermally stable, and biocompatible structures from industry “waste” to value-added products. This work could also enable printing of lignin with other materials into a composite or carbon structure for a range of applications and broaden the functional choices for constructing 3D lignin-based composites that are not applicable in FDM printing. As a biodegradable material from wood, the lignin 3D structure made by ink printing shows great potential to replace plastics for certain applications, which will promote continuous and healthy progress toward sustainability for future engineering of wood-based materials.

3. Experimental Section

Materials and Chemicals: Alkali lignin from hardwood (mainly used and analyzed in this work) was precipitated by H_2SO_4 solution from NaOH cooking spent liquor. Kraft lignin from softwood with molecular weight of 13400 Da was provided by Meadwestvaco Co., Ltd. (Shanghai). Alkali lignin from softwood and kraft lignins from hardwood were purchased from Nanjing Chemical Reagent Co., Ltd. of China. Cellulose with a concentration of 2.74 wt% in water was purchased from Sappi company (North American). Pluronic F127 was purchased from Sigma-Aldrich.

Preparation of Lignin and Cellulose inks: The alkali lignin from hardwood (20 g) was dispersed into deionized water (250 mL) and then subjected the ultrasonication (VC505, Sonics & Materials, Inc.) at 20 kHz frequency for 1 h. The small and ultrafine lignin particles were then obtained after centrifugation (8000 rpm

and 20 min) and freeze-drying. Pluronic F127 was dissolved in deionized water with a concentration of 20 wt% under stirring at 0 °C for 12 h. We then mixed the freeze-dried lignin powder with the F127 aqueous solution at different ratios of 1:0.8, 1:1, 1:1.2, 1:1.4, and 1:1.6 (w/v), and then the mixture was ground in an agate mortar to prepare the lignin inks. The Sappi cellulose was directly vacuum filtered (8 h) to obtain concentrated cellulose ink for direct ink printing, and the water content in cellulose was determined by weighing method after water evaporation at 105 °C.

Direct Ink Printing: Cellulose and lignin inks were printed using a benchtop robot (Fisnar F4200n) and the patterns were controlled by programmed procedures. The inks were sealed in separate syringes and the stainless-steel nozzles were used with different inner diameters of 0.58, 0.66, and 0.84 mm. An air-driven fluid dispenser (DSP501N, Fisnar) provided pressure from 0 to 100 psi to extrude the inks onto a flat glass slide. After printing, the samples were immediately transferred into a freezer at -40 °C and then were placed into a freeze dryer to remove water. The structures of the printed lignin and cellulose scaffolds were then thermally stabilized at 120 °C in muffle furnace under air atmosphere for 2 h. The printability of alkali lignin from softwood and kraft lignins from hardwood and softwood were also determined to demonstrate the universality of this direct ink printing for lignin.

Preparation of Activated Carbon for Water Treatment: The printed grid structure was carbonized at 800 °C for 2 h in argon atmosphere at a heating rate of 5 °C min^{-1} . The carbonized lignin was then immersed in KOH solution for 3 h at 50 °C, the mass ratio of carbonized lignin to activating agent is 2:5. Then the dried material was transferred into nitrogen gas and activated for 2 h at 800 °C. 50 mg of the active materials (activated carbon from printed lignin and commercial activated carbon) were placed into a 50 mL 15 mg L^{-1} MB solution. After 20 min, 1 mL of the MB solution was measured by the UV-vis spectrometer to evaluate the water treatment capacity of activated carbon from printed lignin.

Characterization: The structural differences of alkali lignins from hardwood and softwood were analyzed by ^{13}C nuclear magnetic resonance (NMR). 150 mg of alkali lignin was dissolved in 0.5 mL dimethyl sulfoxide- d_6 (DMSO- d_6). Chromium (III) acetylacetonate

(20 μL , 0.01 M) was added to provide a complete relaxation of all nuclei. The mixture was then characterized on a Bruker AVANCE III 600 MHz spectrometer (Bruker, Switzerland) at room temperature. The rheological properties were measured using a stress-controlled AR 2000 rheometer (TA Instruments). The storage and loss moduli (G' and G'') were measured at a range of 10^{-3} – 10^4 Pa at a constant frequency of 1.0 Hz, and the viscosity was recorded from 10^{-3} to 10^3 s^{-1} . Shape retention capability of the 3D printed lignin structure in the thickness direction was evaluated by comparing the height of printed lignin structure to the theoretical height. The theoretical height was calculated according to the inner diameter of printing nozzle. In order to determine the height of printed pattern by vernier caliper clearly and accurately, a nozzle with the inner diameter of 0.84 mm was used for direct ink printing. The relationship between the printing speed and the required minimum pressure for different inner diameters of needles was also determined. The required minimum pressure is defined as the pressure of enabling the lignin-based ink steadily and continuously extruded from printed nozzle without stacking or breaking.

The morphologies of the printed samples were observed on a scanning electron microscope (SEM, Hitachi SU-70). Water stability of lignin and cellulose scaffolds with the same pattern was characterized by immersing them into water. The transmittance spectra of the printed lignin and cellulose patterns were measured by a UV–vis Spectrometer Lambda 35 equipped with an integrating sphere (PerkinElmer, USA). The MB solution before and after adsorption by activated materials was measured on a Specord 200 UV–vis spectrometer (Analytik Jena AG). The tensile strength of the printed filaments (with the length of 50 mm and diameter of 0.58 mm) was measured on a Tinius Olsen H25KT with a test speed of 2 mm min^{-1} . The compressive strength was tested on an Instron 3367 machine with a constant test speed of 5 mm min^{-1} . The specific surface area was analyzed by N_2 adsorption/desorption at -196 $^\circ\text{C}$ (Autosorb-IQ, Quantachrome, USA) for the printed cellulose and printed lignin before and after thermal stabilization. Before the measurement, all samples were degassed at 80 $^\circ\text{C}$ for 2 h under vacuum. The specific surface area was calculated from the N_2 adsorption isotherm using the Brunauer–Emmett–Teller method. FTIR spectra were recorded by a Thermo Nicolet Nexus 670 FTIR. The thermostability was determined by a thermogravimetric analyzer (SDT 650) with a heating rate of 10 $^\circ\text{C min}^{-1}$ in air atmosphere.

Supporting Information

Supporting Information is available from the Wiley Online Library or from the author.

Acknowledgements

The authors acknowledge the support of the Maryland Nanocenter and its AIM Lab.

Conflict of Interest

The authors declare no conflict of interest.

Author Contributions

B.J., Y.Y., and Z.L. contributed equally to this work. L.H., B.J., and Y.Y. designed the experiments. B.J., Y.Y., and Z.L. analyzed the data. Q.X. and J.G. conducted the UV measurements. B.J., M.J., and R.M. provided the SEM characterization. B.J., Z.L., and X.W. were responsible for the rheology measurements. B.J. and G.C. were conducted the characterization of specific surface area. L.H., B.J., Y.Y., and Z.L. collectively wrote the paper. All authors commented on the final manuscript.

Keywords

3D printing, ink, lignin, structural scaffolds, wood inspired

Received: December 10, 2019

Revised: May 2, 2020

Published online:

- [1] A. Ambrosi, M. Pumera, *Chem. Soc. Rev.* **2016**, *45*, 2740.
- [2] E. MacDonald, R. Wicker, *Science* **2016**, *353*, aaf2093.
- [3] R. L. Truby, M. Wehner, A. K. Grosskopf, D. M. Vogt, S. G. M. Uzel, R. J. Wood, J. A. Lewis, *Adv. Mater.* **2018**, *30*, 1706383.
- [4] S. Ostrovidov, S. Salehi, M. Costantini, K. Suthiwanich, M. Ebrahimi, R. B. Sadeghian, T. Fujie, X. Shi, S. Cannata, C. Gargioli, *Small* **2019**, e1805530.
- [5] K. Fu, Y. Yao, J. Dai, L. Hu, *Adv. Mater.* **2017**, *29*, 1603486.
- [6] X. Tian, J. Jin, S. Yuan, C. K. Chua, S. B. Tor, K. Zhou, *Adv. Energy Mater.* **2017**, *7*, 1700127.
- [7] Y. Yao, K. Fu, C. Yan, J. Dai, Y. Chen, Y. Wang, B. Zhang, E. Hitz, L. Hu, *ACS Nano* **2016**, *10*, 5272.
- [8] X. Wang, M. Jiang, Z. Zhou, J. Gou, D. Hui, *Composites, Part B* **2017**, *110*, 442.
- [9] K. Markstedt, K. Håkansson, G. Toriza, P. Gatenholm, *Appl. Mater. Today* **2019**, *15*, 280.
- [10] R. Wimmer, B. Steyrer, J. Woess, T. Koddenberg, N. Mundigler, in *Int. Conf. on Wood Science and Engineering in the Third Millennium*, Ed. Univ. Transilvania, Brasov **2015**, p. 145.
- [11] T. Li, J. Aspler, A. Kingsland, L. M. Cormier, X. Zou, *J. Sci. Technol. For. Prod. Processes* **2016**, *5*, 30.
- [12] A. J. Ragauskas, G. T. Beckham, M. J. Bidy, R. Chandra, F. Chen, M. F. Davis, B. H. Davison, R. A. Dixon, P. Gilna, M. Keller, P. Langan, A. K. Naskar, J. N. Saddler, T. J. Tschaplinski, G. A. Tuskan, C. E. Wyman, *Science* **2014**, *344*, 1246843.
- [13] F. Jiang, T. Li, Y. Li, Y. Zhang, A. Gong, J. Dai, E. Hitz, W. Luo, L. Hu, *Adv. Mater.* **2018**, *30*, 1703453.
- [14] Y. Li, H. Zhu, Y. Wang, U. Ray, S. Zhu, J. Dai, C. Chen, K. Fu, S. H. Jang, D. Henderson, T. Li, L. Hu, *Small Methods* **2017**, *1*, 1700222.
- [15] D. Cao, Y. Xing, K. Tantratian, X. Wang, Y. Ma, A. Mukhopadhyay, Z. Cheng, Q. Zhang, Y. Jiao, L. Chen, H. Zhu, *Adv. Mater.* **2019**, *31*, 1807313.
- [16] K. Markstedt, A. Mantas, I. Tournier, H. M. Ávila, D. Hägg, P. Gatenholm, *Biomacromolecules* **2015**, *16*, 1489.
- [17] G. Siqueira, D. Kokkinis, R. Libanori, M. K. Hausmann, A. S. Gladman, A. Neels, P. Tingaut, T. Zimmermann, J. A. Lewis, A. R. Studart, *Adv. Funct. Mater.* **2017**, *27*, 1604619.
- [18] J. J. Koh, G. J. H. Lim, X. Zhou, X. Zhang, J. Ding, C. He, *ACS Appl. Mater. Interfaces* **2019**, *11*, 13787.
- [19] X. Zhang, X. Ma, T. Hou, K. Guo, J. Yin, Z. Wang, L. Shu, M. He, J. Yao, *Angew. Chem., Int. Ed.* **2019**, *58*, 1.
- [20] A. J. Benitez, J. Torres-Rendon, M. Poutanen, A. Walther, *Biomacromolecules* **2013**, *14*, 4497.
- [21] W. G. Glasser, R. A. Northey, T. P. Schultz, in *ACS Symp. Series*, American Chemical Society, Washington, D.C. **1999**.
- [22] P. Figueiredo, K. Lintinen, J. T. Hirvonen, M. A. Kostianen, H. A. Santos, *Prog. Mater. Sci.* **2018**, *93*, 233.
- [23] Q. Sun, R. Khunsupat, K. Akato, J. Tao, N. Labbé, N. C. Gallego, J. J. Bozell, T. G. Rials, G. A. Tuskan, T. J. Tschaplinski, A. K. Naskar, Y. Pu, A. J. Ragauskas, *Green Chem.* **2016**, *18*, 5015.
- [24] C. D. Tran, J. Chen, J. K. Keum, A. K. Naskar, *Adv. Funct. Mater.* **2016**, *26*, 2677.
- [25] N. A. Nguyen, S. H. Barnes, C. C. Bowland, K. M. Meek, K. C. Littrell, J. K. Keum, A. K. Naskar, *Sci. Adv.* **2018**, *4*, eaat4967.

- [26] S. K. Bhatia, K. W. Ramadurai, *3D Printing and Bio-Based Materials in Global Health*, Springer Briefs in Materials, Springer, New York **2017**, Ch. 3.
- [27] K. Akato, C. D. Tran, J. Chen, A. K. Naskar, *ACS Sustainable Chem. Eng.* **2015**, 3, 3070.
- [28] P. Song, Z. Cao, Q. Meng, S. Fu, Z. Fang, Q. Wu, J. Ye, *J. Macromol. Sci., Part B* **2012**, 51, 720.
- [29] B. Wu, S. Li, J. Shi, S. Vijayavenkataraman, W. Lu, D. Trau, J. Fuh, *Bioprinting* **2018**, 12, e00030.
- [30] W. Herschel, B. Bulkley, *Kolloid* **1926**, 39, 291.
- [31] J. A. Lewis, *Adv. Funct. Mater.* **2006**, 16, 2193.
- [32] C. Crestini, H. Lange, M. Sette, D. S. Argyropoulos, *Green Chem.* **2017**, 19, 4104.
- [33] A. Sosnik, D. Cohn, *Biomaterials* **2005**, 26, 349.
- [34] D. Cohn, A. Sosnik, S. Garty, *Biomacromolecules* **2005**, 6, 1168.
- [35] A. Tejado, C. Pena, J. Labidi, J. M. Echeverria, I. Mondragon, *Bioresour. Technol.* **2007**, 98, 1655.
- [36] R. Ding, H. Wu, M. Thung, N. Bowler, M. R. Kessler, *Carbon* **2016**, 100, 126.
- [37] Y. Zhang, J. Wu, H. Li, T. Yuan, Y. Wang, R. Sun, *ACS Sustainable Chem. Eng.* **2017**, 5, 7269.
- [38] O. Gordobil, R. Moriana, L. Zhang, J. Labidi, O. Sevastyanova, *Ind. Crops Prod.* **2016**, 83, 155.
- [39] B. Jiang, C. Chen, Z. Liang, S. He, Y. Kuang, J. Song, R. Mi, G. Chen, M. Jiao, L. Hu, *Adv. Funct. Mater.* **2019**, 29, 1906307.
- [40] B. M. Upton, A. M. Kasko, *Chem. Rev.* **2016**, 116, 2275.
- [41] Z. Sun, B. Fridrich, A. de Santi, S. Elangovan, K. Barta, *Chem. Rev.* **2018**, 118, 614.
- [42] N. Supanchaiyamat, K. Jetsrisuparb, J. T. N. Knijnenburg, D. C. W. Tsang, A. J. Hunt, *Bioresour. Technol.* **2019**, 272, 570.